JOM, Vol. 67, No. 4, 2015
DOI: 10.1007/s11837-015-1364-1
© 2015 The Minerals, Metals & Materials Society

Sol–Gel Derived Hydroxyapatite Coating on Mg-3Zn Alloy for Orthopedic Application

SANJAY SINGH,[1,2] R. MANOJ KUMAR,[1,2] KISHOR KUMAR KUNTAL,[1,3] PALLAVI GUPTA,[1,3] SNEHASHISH DAS,[4] R. JAYAGANTHAN,[2,3] PARTHA ROY,[4] and DEBRUPA LAHIRI[1,2,3,5,6]

1.—Biomaterials and Multiscale Mechanics Laboratory, Indian Institute of Technology Roorkee, Roorkee 247667, Uttrakhand, India. 2.—Department of Metallurgical and Materials Engineering, Indian Institute of Technology Roorkee, Roorkee 247667, Uttrakhand, India. 3.—Centre of Nanotechnology, Indian Institute of Technology Roorkee, Roorkee 247667, Uttrakhand, India. 4.—Molecular Endocrinology Lab, Department of Biotechnology, Indian Institute of Technology Roorkee, Roorkee 247667, Uttrakhand, India. 5.—e-mail: debrupa.lahiri@gmail.com. 6.—e-mail: dlahifmt@iitr.ac.in

In recent years, magnesium and its alloys have gained a lot of interest as orthopedic implant constituents because their biodegradability and mechanical properties are closer to that of human bone. However, one major concern with Mg in orthopedics is its high corrosion rate that results in the reduction of mechanical integrity before healing the bone tissue. The current study evaluates the sol–gel–derived hydroxyapatite (HA) coating on a selected Mg alloy (Mg-3Zn) for decreasing the corrosion rate and increasing the bioactivity of the Mg surface. The mechanical integrity of the coating is established as a function of the surface roughness of the substrate and the sintering temperature of the coating. Coating on a substrate roughness of 15–20 nm and sintering at 400°C shows the mechanical properties in similar range of bone, thus making it suitable to avoid the stress-shielding effect. The hydroxyapatite coating on the Mg alloy surface also increases corrosion resistance very significantly by 40 times. Bone cells are also found proliferating better in the HA-coated surface. All these benefits together establish the candidature of sol–gel HA-coated Mg-3Zn alloy in orthopedic application.

INTRODUCTION

In recent years, biodegradable materials are highly researched for orthopedic application because of their advantage in avoiding additional surgery for the removal of an implant.[1] In this connection, magnesium has been considered as a pioneer material for orthopedic application. In addition to its biodegradability, Mg is also attractive for this purpose due to its light weight (density = 1.74–2 g/cm^3) and mechanical properties more similar to human bone, compared with currently used orthopedic materials, viz., Co-Cr alloy, Ti alloy and stainless steel.[2] Mg has an elastic modulus (41–45 GPa), a fracture toughness (15–40 MPam$^{1/2}$), and the compressive strength (65–100 MPa) most close to those of natural bone (density = 1.8–2.1 g/cm^3, E = 3–20 GPa, fracture toughness = 3–6 MPam$^{1/2}$, and compressive strength = 130–180 MPa).[3–5] The similarity in mechanical properties between bone and implant material is very much essential to avoid the stress-shielding effect, which otherwise leads to a reduction in the density and stability of bone, as well as a decrease in new bone growth.[6] In addition, it is also found that Mg is a vital element of natural bone and helps in the regeneration of the same.[7]

The main issue with Mg is its high corrosion rate in the bioenvironment with chloride ions, which causes metal dissolution and evolution of hydrogen gas, leading to loss of mechanical strength of the implant before healing of bone.[8] Many efforts have been made to reduce the corrosion rate of magnesium. Alloying can improve corrosion resistance and mechanical strength of Mg-based alloys.[9] There are mainly two broad categories of Mg alloys available in commercial use. The first one is AZ series, which contains up to 10% of aluminum along with trace amount of zinc and manganese and the second one

(Published online March 17, 2015)

has rare earths (REs) as the alloying elements along with zinc, yttrium, and sometimes zirconium.[10] However, these alloys might not be suitable for orthopedics. Because of the alloying of aluminum, there is a possibility of dementia and Alzheimer's disease. Moreover, it is also harmful to neurons.[11] Excessive addition of rare earth element, such as yttrium, modifies genes and shows an adverse effect on DNA transcription factor.[12] Therefore, alloying of Al and RE elements is unsuitable for biomedical application when alloyed above 10%.[13] Hence, there is need to develop a novel magnesium alloy for biomedical application. Zinc is one of the most abundantly present elements in the human body.[14] According to the Mg-Zn phase diagram,[15] the maximum solubility of Zn in Mg is 6.2%. Furthermore, it increases the corrosion resistance and mechanical properties of magnesium alloys.[16] It has also been reported that the Mg-3Zn alloy exhibits the lowest degradation rate and highest corrosion resistance due to the presence of a higher amount of MgZn intermetallic phase.[17] Therefore, in this study Mg-3Zn alloy has been chosen as a substrate.

However, even after alloying with high potential elements such as Zn, RE, Al, etc., the corrosion rates of Mg alloys are still significant,[10,18] necessitating some kind of surface treatment using an appropriate coating to reduce the degradation rate for orthopedic application. The best material to make a coating is the one that can give some positive contribution to the bioactivity in addition to increasing the corrosion resistance. A bioactive material for orthopedic application should be able to form bone-like apatite surrounding itself when exposed to the body environment.[19] Hydroxyapatite ($Ca_{10}(PO_4)_6(OH)_2$) has been used extensively in orthopedic applications because of its ability to form a direct chemical bond with living tissues.[20] Of all the calcium phosphate compounds, hydroxyapatite is the most stable compound in the physiological environment accompanied by exceptional biocompatibility because of its compositional similarity (Ca/P equals to 1.67) with the natural bone.[21] However, due to the poor mechanical properties of hydroxyapatite (HA), such as brittleness and low fracture toughness, it cannot be used for load bearing application.[22] Therefore, by applying HA coating on metallic implant, it is possible to combine the mechanical benefits of metal alloys with bioactivity at the bone-implant interface. Hydroxyapatite coating on metal implant helps for fast regeneration of bone as well apatite formation on its surface in a body environment. Being ceramic, HA has high corrosion resistance. Thus, the coating of HA acts as a barrier between magnesium alloy substrate and body fluid and protects magnesium alloy from high corrosion rate and ensures a good mechanical integrity of the implant. Gradual degradation of the coating after implantation increases the degradation time of magnesium alloy and can make it a perfect constituent for an ideal degradable implant.

Several coating techniques have been used to prepare a hydroxyapatite coating on magnesium alloys,[23] namely, hydrothermal deposition,[24–26] biomimetic method,[27,28] electrophoretic deposition,[29–31] and sol–gel method.[32–35] The plasma spray deposition technique has been used worldwide for other metallic implants, like stainless steel and titanium. However, due to the high temperature involved in the process, a phase change of hydroxyapatite and a change in the characteristics of metallic substrate were found. Furthermore, Mg has a low melting point so the plasma spray coating cannot be used. Among all these techniques, the sol–gel method has received more attention because it is inexpensive and environmentally friendly, and it can coat complex surfaces, which is a must for typical implant shapes.[36] It can also better control the chemical composition and prepare the homogeneous coating.[37] Researchers have used sol–gel techniques to synthesize HA coating on different Mg alloys of mainly AZ series.[32,33,38] These studies have mainly focused on the corrosion behavior and adhesion of the coating to a substrate. Rojaee et al.[33] found that an intercept of the anodic and cathodic curve showed the shifting of current density and potential to more noble values. The corrosion current density was decreased by 7.8 times and the corrosion potential was increased by 1.07 times. It could be a good indication of the stability of the HA coating on Mg alloys. On the other hand, an immersion test was done for different time periods. The immersion test reveals the nucleation of apatite on the HA coating. Therefore, it showed that HA coating prompts biomineralization. A peel-off test was conducted by researchers to measure the bonding strength between the coating and the substrate. The results showed that bonding strength increases with increase in temperature.[32] Rojaee et al.[33] investigated the sol–gel HA coating on AZ91 alloy. The adhesion strength was in range of 4.2 ± 0.3 MPa.

The surface roughness of the substrate can also influence the coating morphology. Surface roughness not only provides wettability of HA solution on substrate but also is responsible for mechanical interlocking between coating and substrate. For dip coatings, if the main mechanism of adhesion is mechanical interlocking to the surface, then the roughness plays an important role in determining the mechanical integrity of the coating on the substrate during operation. On the other hand, if the surface roughness of the substrate is greater, then it can lead to stress concentration and crack propagation in the coating. Therefore, it is necessary to optimize the surface roughness. The mechanical integrity of the coating is also a major issue because sol–gel-derived HA coatings are very porous. Therefore, it is necessary to check the mechanical integrity of the coating. However, as per the authors' knowledge, the literature is scarce on the evaluation of the effect of surface roughness on the morphology of sol–gel HA dip coating on the Mg substrate. Fur-

thermore, there is no reported study so far evaluating the mechanical properties of such coatings.

In the current study, hydroxyapatite is coated on a Mg-3Zn magnesium alloy using the sol–gel technique to improve the bioactivity and biodegradation. The mechanical integrity of the coating as a function of heat treatment and surface roughness of the substrate is investigated. The corrosion behavior of the prepared sample in simulated body fluid (SBF) solution was investigated to analyze the effectivity of sol–gel HA coating on Mg alloy for orthopedic application. In addition to all these, the sol–gel HA-coated Mg alloy surface is also evaluated for its biocompatibility through in vitro studies assessing the proliferation and viability of bone cells. These results are very important for establishing the application of the above-discussed material system in orthopedics and have not been reported in the literature so far.

MATERIALS AND METHODS

Synthesis of Hydroxyapatite Coating

In the current study, an as-cast Mg-3Zn alloy (Exclusive Magnesium Private Limited, Hyderabad, India) containing 3 wt.% zinc was used as a substrate material. Mg (99.9% purity) and Zn (99.9% purity) were melted in resistance-type furnace in a temperature range of 680–730°C under an argon atmosphere and stirred for 3 min at a regular interval of 15 min to obtain a homogenized structure. A gravity die casting process was used for casting purposes. The molten material was poured in a cast iron die mold with the dimensions of $500 \times 90 \times 60$ mm^3 and cooled down. The ingots were cut into coupons measuring $15 \times 15 \times 3$ mm^3 for coating and for the following studies. The surfaces of the coupons were metallographically prepared by successively polishing with silicon carbide papers up to 1200 grit and 2000 grit to observe the effect of surface roughness. These polished samples were cleaned ultrasonically in acetone and distilled water for 15 min and 20 min to avoid surface contamination.

HA coating was prepared on a substrate using the combination of the sol–gel and dip coating techniques. HA solution was prepared by adding calcium nitrate tetrahydrate ($Ca(NO_3)_2{\cdot}4H_2O$) and phosphorus pentaoxide (C_2H_5OH) in ethanol separately. A calcium precursor was added in a phosphorus precursor dropwise to obtain a homogenous solution with a Ca/P ratio of 1.67. The prepared solution was stirred on a magnetic stirrer at 400 rpm for 5 h at room temperature in a closed beaker. Finally, the prepared samples were dipped vertically and withdrawn from the prepared sol at a rate of 1 mm/s. Sol-coated samples were kept at room temperature for 24 h so that the aging process could be completed.[39] Then, the aged samples were dried by heating to 60°C for 1 h in a hot-air oven and finally the samples were sintered at 300°C and 400°C for 4 h at a heating rate of 2°C/min followed by furnace cooling in customized tube furnace. Four types of samples were prepared. In the first two, the samples were polished up to 1200 grit and then sintered at 300°C and 400°C. Later, two were polished up to 2000 grit sintered at 300°C and 400°C, which will be referred as 12-300, 12-400, 20-300, and 20-400 further in this study.

To determine the crystallinity of HA, the solution was also dried at 60°C and followed by sintering at 300°C and 400°C for 2 h to get the powder for x-ray diffraction (XRD) analysis. This was done because the coating was very thin, and it would not give significant HA peaks compared with the intensity of that of Mg peaks in normal XRD studies.

Physical Characterization of Powder and Coating

The characterization of hydroxyapatite coating and calcined powder was done using a scanning electron microscope (SEM; EVO 18 special edition, Carl Zeiss, Oberkochen, Germany) and an x-ray diffractometer (Smart Lab, Rigaku, Japan). The XRD analysis was run at 2θ range of 20°–80° with a scan rate of 1°/min by using Cu Kα (λ = 1.5418 Å) radiation. The peak broadening of the XRD pattern can be used to determine the crystallite size in a direction perpendicular to crystallographic plane by using Scherrer's formula as follows:[40]

$$X = \frac{0.9\lambda}{\beta \cos\theta} \tag{1}$$

where X, λ, β, and θ are crystallite size (nm), wavelength of x-ray (in nm), and full width at half maximum (radian) for the diffraction peak under consideration and diffraction angle (degree), respectively.

The surface morphology and microstructure of the coating before corrosion and after corrosion were observed using a scanning electron microscope.

Potentiodynamic Polarization Study

An electrochemical investigation of HA-coated Mg-3Zn alloys was performed to assess its corrosion behaviour in SBF at 37 ± 1°C with the three-electrode cell having standard platinum wire as a counterelectrode and KCl-saturated Ag/AgCl electrode as a reference electrode, respectively. All the experiments were carried out using potentiostat/galvanostat (Interface 1000; Gamry instruments Inc., Warminster, PA). Before the experiment, the samples were stabilized at their open circuit potential (OCP) for 30 min. The potentiodynamic polarization tests were performed from −250 mV versus OCP to 250 mV versus Ag/AgCl with a scan rate of 1 mV/s. The corrosion potential (E_{corr}) and corrosion current density (I_{corr}) were calculated by using the Tafel extrapolation method.

Mechanical Characterization

A nanoindentation test was carried out using Hysitron TI950 triboindenter (Hysitron Inc., Eden Prairie, MN) equipped with a three-sided pyramid Berkovich diamond indenter with a tip radius of 100 nm to measure the hardness and elastic modulus of the coating. The load was applied at the rate of 6.25 μN/s up to the maximum load of 50 μN/s and a dwell at peak load for 1 s, followed by unloading at same rate as loading. A minimum of 25 indents were taken on each coating with different places to represent the coating hardness (H) and reduced elastic modulus (E_r). The values were calculated from the graph load versus depth of penetration of the indents using the slope of unloading part as per the Oliver–Pharr method.[41]

Biocompatibility and Cell Culture Test

The human osteosarcoma cell line MG-63 was procured from the National Centre for Cell Science (Pune, India) under cell culture conditions. After preincubation in SBF and Dulbecco's modified eagle's medium (DMEM) cell culture medium, all the samples were transferred into a 24-well plate (one sample per well). For cell adhesion, MG63 cells were trypsinized, centrifuged, and afterward resuspended in DMEM medium to a concentration of 1×10^6 cells per mL. Then, 50 μL of the cell suspension was homogeneously applied onto each bare and coated sample. The samples were incubated for 4 h to allow the study of initial cell adhesion. Cell viability was assessed via MTT assay. All tests were performed in triplicate. For MTT assay 0.5 mg/mL of tetrazolium salt solution (MTT), 3-[4,5-dimethylthiozol-2-yl]-2,5 diphenyltetrazolium bromide (Himedia, Mumbai, India) was added to each sample for 4 h at 37°C and kept in a CO_2 incubator after 1 and 3 days of incubation. Cell viability was assessed by quantification of water-insoluble dark blue crystals of formazan precipitate formed after a reduction of yellow water-soluble MTT dye by mitochondrial enzyme succinic dehydrogenase. Only viable cells contain this enzyme. After incubating for 4 h, complete solubilization of insoluble formazan crystals was also done by adding 1 mL ethanol-dimethyl sulfoxide (Amresco, Solon, OH) solution (1:1). Prior to this, the cell culture medium was removed from each well. The absorbance was measured at 570 nm for all the samples along with controls containing no cells with the help of ultraviolet–visible double-beam spectrophotometer (Lasany, Haryana, India).

RESULTS AND DISCUSSION

Physical Properties Evaluation of Powder and Coating

The morphology of the synthesized HA particles obtained after sintering at 300°C and 400°C for 4 h is shown in (Fig. 1a and b), respectively. Spherical-shaped particles were observed, which are typical for sol–gel-derived hydroxyapatite. The HA powder heat treated at a higher temperature shows a larger particle size due to higher diffusion and growth of crystals. The average particle size is found to be in the range of 31–58 nm and 44–80 nm for powder sintered at 300°C and 400°C, respectively.

Figure 2a and b presents the XRD pattern of dried gel heat treated at 300°C and 400°C. The XRD pattern of powder sintered at 300°C exhibits very low crystallinity, which is denoted by the absence of significantly sharp peaks. As the temperature increases to 400°C, it shows peaks of HA (JCPDS#24-0033). The broadening of peak (002) was chosen because it was sharp and did not overlap with other peaks. The crystallite size of hydroxyapatite was calculated to be 42 nm using Scherrer's equation. As the crystallinity was achieved at 400°C, this temperature was chosen to treat the coatings, keeping in mind the low meting point of Mg-3Zn alloy, as well as to avoid the chance of its reaction with oxygen.[42]

The morphology of the Mg-3Zn substrate, polished up to 1200 and 2000 grit silicon carbide emery paper, is presented in Fig. 3a and b. The surface of Mg-3Zn substrate polished up to 1200-grit emery has much higher roughness than the one polished up to 2000-grit emery paper. The surface roughness (R_a), as recorded using a contact profilometer, are in the range of 130–150 nm and 15–20 nm for 1200 and 2000 grit, respectively.

The effect of roughness of Mg-3Zn alloy on the hydroxyapatite coating is shown in Fig. 4.

Figure 4a and b shows the surface morphology of hydroxyapatite coated Mg-3Zn substrate having roughness of 15–20 nm and 130–150 nm, sintered at 300°C and Fig. 4c and d for the same surfaces sintered at 400°C, respectively. It was conceived from the XRD results of sintered HA powders that the coatings sintered at 400°C would have higher crystallinity, and the ones treated at 300°C would show very low crystallinity. HA coating done on a substrate having lower roughness (Fig. 4a and c) shows that the smooth coating has very few cracks compared with the coating on a substrate with higher roughness (Fig. 4b and d). High roughness produced by 1200-grit emery paper engages a relatively higher volume of HA to be deposited on surface, which results in crack initiation due to high shrinkage during drying and sintering. Also, the sharp corners of the rough surface act as a stress concentrator due to which stress accumulates in the coating and results in crack propagation in the coating. The effect of sintering temperature on the shrinkage can be seen in Fig. 4b and d. It is found that the cracks are more prominent in the coating sintered at 400°C as shown in Fig. 4d as compared with the crack showed in Fig. 4b at 300°C, although the surface roughness values of both were same. It can be explained that more shrinkage occurs in the coating at a higher temperature, leading to more prominent cracks.

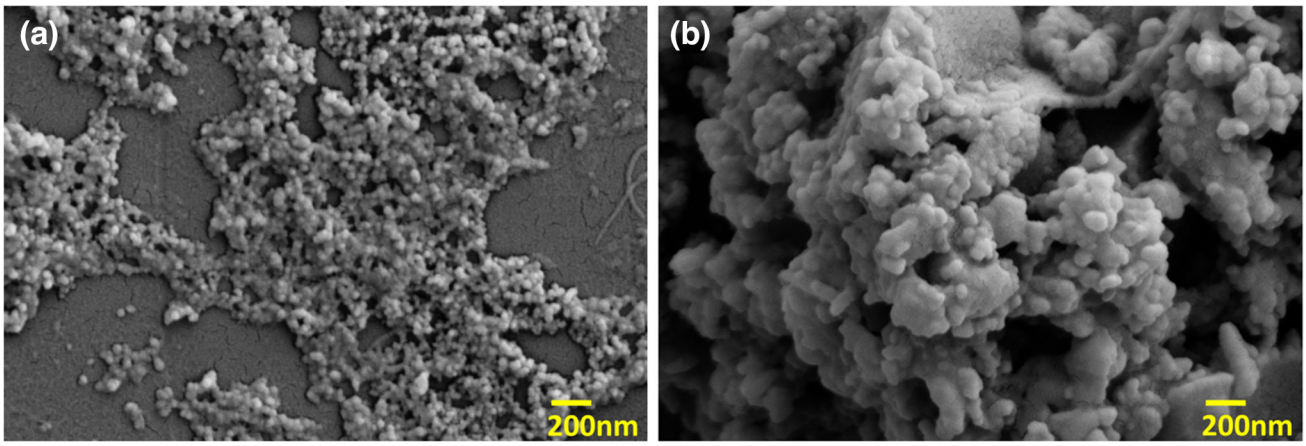

Fig. 1. SEM micrograph of HA powder sintered at (a) 300°C and (b) 400°C.

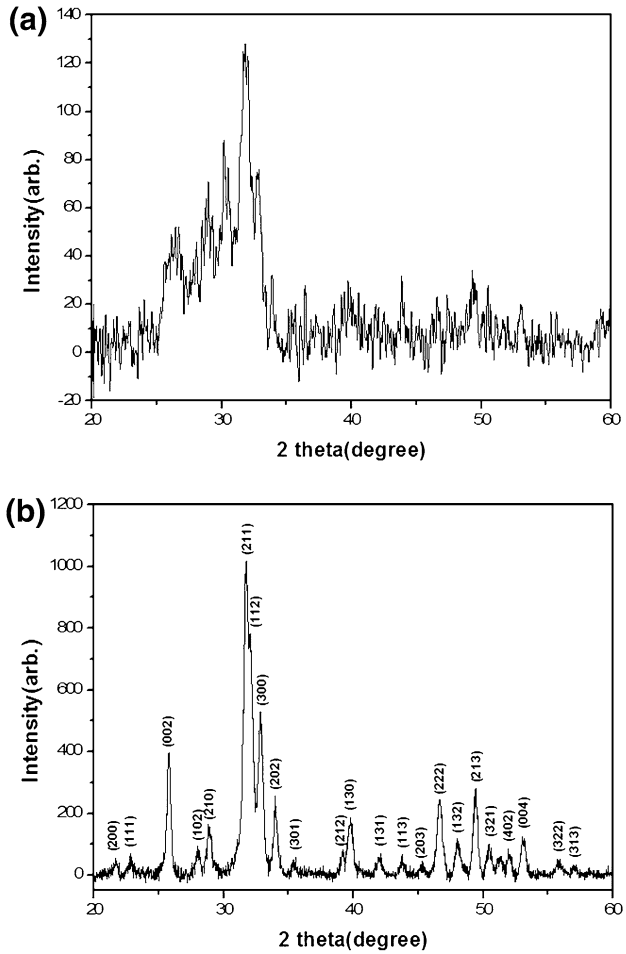

Fig. 2. X-ray diffraction pattern of the sol–gel derived HA powder after heat treatment at (a) 300°C and (b) 400°C.

SEM micrographs of cross section of coated samples are presented in Fig. 5. Figure 5a–d show the cross-section images of 20-300, 12-300, 20-400, and 12-400 HA-coated samples, respectively. The coating thickness of 20-300 and 20-400 samples were 4.7 ± 0.728 μm and 7.1 ± 0.753 μm, whereas the coating thicknesses of 12-300 and 12-400 were 10.2 ± 1.224 μm and 9.1 ± 0.924 μm. It can be seen that Fig. 5b and d are thicker than Fig. 5a and c. This is due to the higher roughness of substrate in Fig. 5b and d. The 20-400 HA coating (Fig. 5c) shows a strong interface with the Mg alloy substrate without any signs of delamination. However, the 20-300 coating (Fig. 5a), which also has low surface roughness (15-20 nm) but is sintered at a lower temperature (300°C), shows a clear sign of delamination with the substrate. The reason for this delamination could be that a lower temperature causes low crystallinity and thus easy detachment of coating from the substrate due to poor mechanical integrity. Both the coatings on rougher surface, 12-300 and 12-400, show a significantly different morphology with greatly disturbed arrangement of the HA structure. The disturbance in the structure is caused by high roughness of the surface, creating more stress in the coating. At the same time, more thickness of these two coatings also indicates a greater volume of HA deposition, which has been discussed before as a source of prominent cracks (Fig. 4) developing on these two. Therefore, lower roughness of about 15–20 nm can be considered as better for obtaining a uniform and crack-free coating. Further optimization is possible in this regard to get an idea about the ideal surface finish for sol–gel HA coating on Mg substrate.

Mechanical Properties of Coating

The mechanical properties of hydroxyapatite coated substrates were analyzed by three sided pyramid Berkovich diamond indenter, which is considered as one of the most suitable methods to analyze the mechanical properties of the thin brittle coating.[43] Figure 6 presents the representative load versus displacement plots for the HA coatings in all the four combinations of surface roughness and sintering temperature. The calculation of elastic modulus and hardness of each coating is done from these studies, which are presented in Table I. The

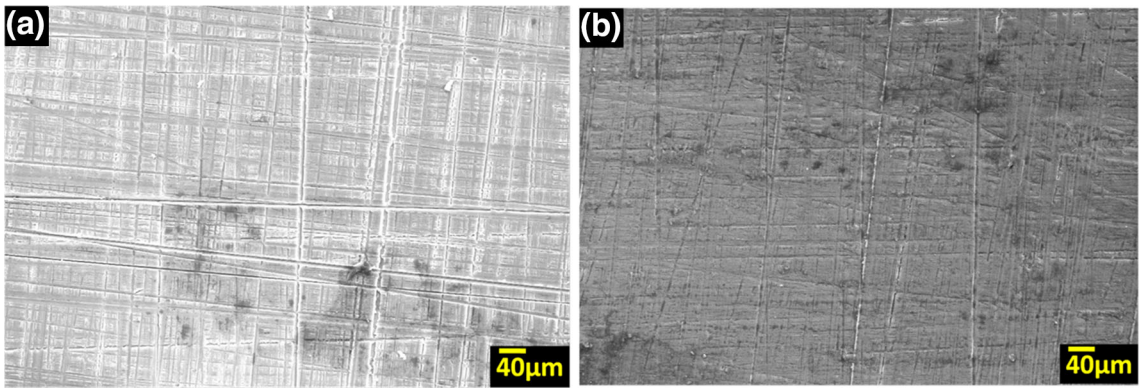

Fig. 3. SEM micrograph of Mg-3Zn substrate polished up to (a) 1200-grit emery paper and (b) 2000-grit emery paper.

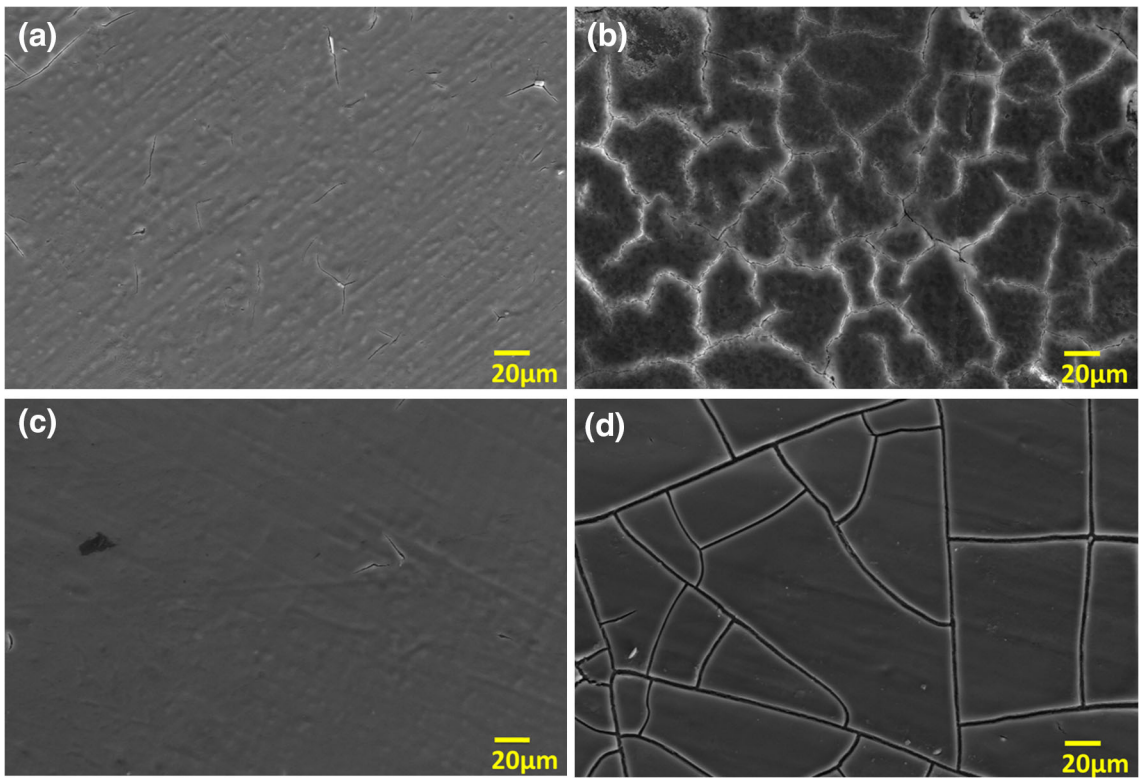

Fig. 4. SEM micrograph of HA-coated sample sintered at 300°C having roughness of (a) 15–20 nm and (b) 130–150 nm. SEM micrograph of HA-coated sample sintered at 400°C having roughness of (c) 15–20 nm and (d) 130–150 nm.

hardness and elastic modulus values for 12-300 and 12-400 were the least, which could be due to the formation of cracks that result in poor cohesion. The hardness and elastic modulus values reported for 20-300 samples were 1.23 ± 0.0738 GPa and 15.18 ± 1.06 GPa. The coating shows lower value of hardness due to its poor internal cohesion.[44] At the same time, it is amorphous at 300°C, so they easily dissolve in a physiological environment;[45] thus, it cannot be used for orthopedic application. As we increase the sintering temperature to 400°C, the hardness and elastic modulus both increase by 7.3% and 52.5%. The E and H values, obtained for these sol–gel dip coatings, are still much lower than those for the coatings synthesized by the pulsed laser-deposition technique done on titanium substrates.[44] The E and H values for coatings done on titanium were 93 GPa and 1.6 GPa, respectively, when sintered at 460°C. The reason for lower hardness and elastic modulus could be the lower sintering temperature of 400°C in the current sol–gel coating.

A second reason for difference in elastic modulus of the HA coating in the current study with above-mentioned pulse laser deposition[44] might be the mechanical properties of the underlying substrate also, which is much more in case of pulse laser

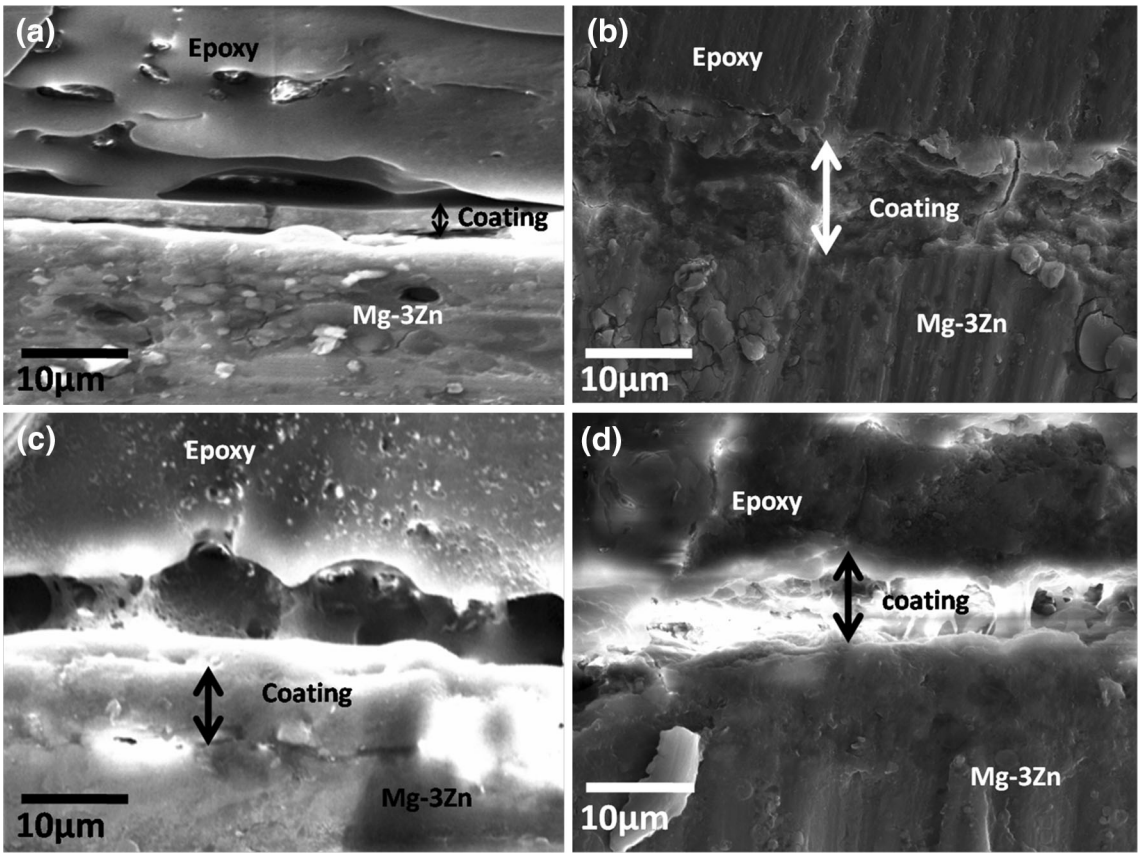

Fig. 5. SEM micrograph of cross section of HA-coated sample sintered at 300°C having roughness of (a) 15–20 nm and (b) 130–150 nm. SEM micrograph of cross section of HA coated sample sintered at 400°C having roughness of (c) 15–20 nm and (d) 130–150 nm.

coating (Ti alloy), as mentioned here (Mg-alloy). If the substrate is not rigid enough, then with the increase of load it will increase the probability of crack formation, which results in lower hardness.[46] However, coating via the sol–gel route can be more attractive for applying the HA coating on Mg-based orthopedic implants, due to multiple reasons; namely, it is an easy and industrial process that can be applied to complex shape design. Also, it is a low-temperature process that can be safely applied to low melting substrates (e.g., Mg).

Because the 20-400 HA coatings have a better hardness and elastic modulus, the fracture toughness of this coating is also studied using the Vickers microhardness indentation technique and Anstis' equation[47] In this technique, the test was carried out using a microhardness tester (Walter UHL, technische mikroskopie, GmbH & Co. KG, Aßlar, Germany), which uses Vickers' probe. A load of 0.98 N was applied on the coating and the dwell time of 15 s. Five indents were made on coatings at different locations. Fracture toughness (K_{IC}) is calculated using the following equation:[47]

$$K_{IC} = 0.016\left(\frac{E}{H}\right)^{\frac{2}{5}}\left(\frac{P}{C^{\frac{3}{2}}}\right) \quad (2)$$

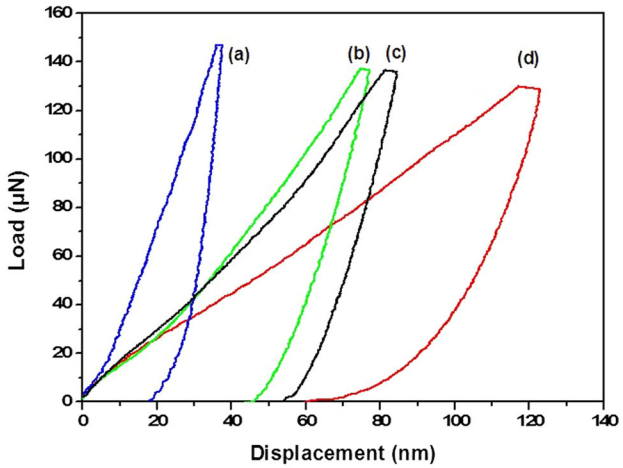

Fig. 6. Load-displacement curves for indentations into a sol–gel–derived HA coating on Mg-3Zn substrate having roughness of 15–20 nm and sintered at (a) 400°C and (b) 300°C. Load–displacement curves for indentations into a sol–gel–derived n-Hap coating on Mg-3Zn substrate having roughness of 130–150 nm and sintered at (c) 400°C and (d) 300°C.

where K_{IC}, E, H, P, and C are the fracture toughness, elastic modulus (GPa), Vickers hardness (GPa), applied load, and radial crack length on the

Table I. Hardness and elastic modulus of hydroxyapatite-coated substrate

Samples	Hardness (GPa)	Elastic Modulus, (GPa)
20-400	1.32 ± 0.105	23.15 ± 1.95
20-300	1.23 ± 0.0738	15.18 ± 1.06
12-400	0.512 ± 0.039	12.69 ± 1.04
12-300	0.43 ± 0.021	11.08 ± 0.715
Mg-3Zn	0.4759 ± 0.025	44 ± 1.89
HA-coated Ti substrate (290°C, PL)	0.55–1.06 (Ref. 43)	74.4–107 (Ref. 43)
HA-coated Ti substrate (460°C, PL)	1.6 (Ref. 43)	93 (Ref. 43)
Cortial bone	–	7–30 (Ref. 48)

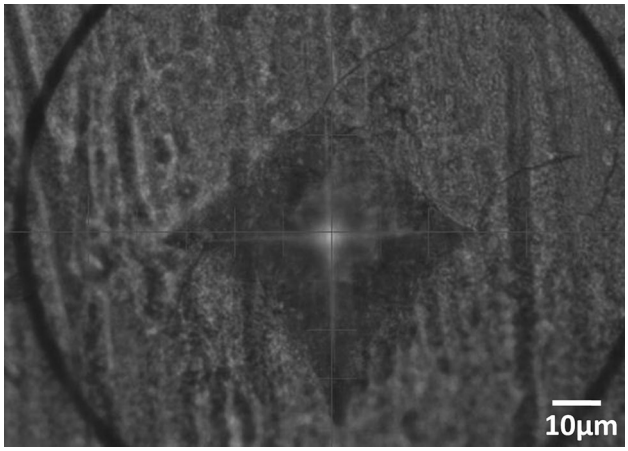

Fig. 7. Optical micrograph of Vickers indentation and cracks in 20-400 HA coating at 0.98 N.

indent, respectively. Figure 7 shows the optical image of the Vickers indentation on 20-400 HA coating. The fracture toughness value for 20-400 samples obtained was 0.49 ± 0.108 MPa/m$^{1/2}$.

Another encouraging fact is that the elastic modulus of the 20-400 HA coating obtained is in the similar range of that of human bone. One reason for using Mg alloys for orthopedic application is to take advantage of its mechanical properties, which are similar to that of human bone and thus scale down the stress-shielding effect. Thus, synthesizing a coating on a surface with a much higher elastic modulus and hardness would nullify the efforts taken in using Mg for reducing the stress-shielding effect. Considering this, the sol–gel HA coating with optimized synthesis conditions can perform the best from a mechanical compatibility point of view. In addition, the presence of a high (35%) amount of porosity in the coating would help in bone ingrowth and better integration of the new bone with implant during in vivo exposure.

Electrochemical Evaluation

From the SEM and mechanical analysis, it can be concluded that coating fabricated on substrate with higher roughness facilitates crack propagation accompanied with lower hardness and elastic modulus. So these samples are not suitable for biomedical applications. Therefore, corrosion studies were performed on substrates with lower surface roughness values.

The protective properties of hydroxyapatite coated Mg-3Zn substrates and bare substrate are shown by electrochemical polarization curve in Fig. 8. The values of corrosion potential (E_{corr}) and corrosion current density (I_{corr}) were directly measured from the polarization curve using the Tafel extrapolation method,[49] and the results are shown in Table II. All the HA-coated samples sintered at different temperatures show higher corrosion resistance than the bare Mg alloy substrate, as reflected from their higher corrosion potential and lower corrosion current density. It can be seen that the samples (20–300°C) show corrosion potential of –0.493 V and corrosion current density of 6.403 μA/cm^2. Compared with the bare sample (E_{corr} of –1.69 V and I_{corr} of 135 μA/cm^2), the E_{corr} of 20-300 is increased by 3.5 times and I_{corr} is decreased by 21 times. Increasing the temperature to 400°C, I_{corr} showed a great decrease by 40 times and E_{corr} is increased by 3.84 times when compared with the bare samples but higher than that of sample 20-300. The E_{corr} of 20-400 increases by 1.12 times and I_{corr} decreases by 1.9 times when compared to the 20-300 samples. With the increase in sintering temperature, the coating is sintered better and becomes more compact and dense, which improves the corrosion resistance by preventing easy access of chloride ions to the Mg alloy substrate. These results clearly demonstrate that HA coating acts as a corrosion inhibitor on the Mg surface in the SBF environment.

The SEM micrographs of bare and 20-400 samples after accelerated corrosion test are shown in (Fig. 9a and b) to understand the corrosion behavior of coated and uncoated samples more thoroughly. It can be clearly observed that apatite has precipitated on both the surfaces, which is expected as the testing is performed in SBF. However, the morphology of the precipitates is very different in bare and dip-coated Mg surfaces. The precipitates on bare Mg-alloy surface form small chunks with very prominent cracks separating them (Fig. 9a). In addition, chipping also occurs in this layer (Fig. 9a), making the bare Mg-alloy surface exposed to a corrosion attack. On the contrary, due to the presence of HA on the surface of the dip-coated sample, the precipitated apatite gets integrated with the coating rather than remaining as separate entity (Fig. 9b). Thus, a negligible amount of cracks and asperities is observed in coated samples, with no chipping and alloy surface exposure. Such morphology has the potential to reduce corrosive attack, especially

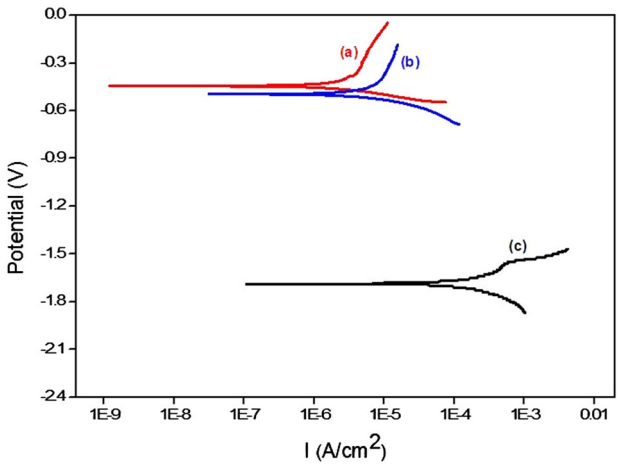

Fig. 8. Representative potentiodynamic polarization curves of sol–gel-derived HA coated Mg-3Zn specimen with roughness of 15–20 nm and sintered at (a) 400°C, (b) 300°C, and (c) bare Mg-3Zn specimen in SBF electrolyte at 37°C ± 1°C.

Table II. Corrosion potential and corrosion current density of hydroxyapatite coated substrate and bare substrate in SBF at 37°C ± 1°C

Sample	E_{corr} (V)	I_{corr} (μA/cm^2)
Bare Mg-3Zn	−1.69 ± 0.086	135 ± 5.33
HA-coated Mg-3Zn (20-300°C)	−0.493 ± 0.0346	6.403 ± 0.45
HA-coated Mg-3Zn (20-400°C)	−0.44 ± 0.032	3.358 ± 0.17

localized attack due to prevention of microgalvanic cell formation. Because of the significant decrease in corrosion resistance, mechanical strength of magnesium implant can be maintained during the healing process.

Evaluation of Biocompatibility

Cell adhesion and a viability assay were done on HA-coated Mg-alloy (20-400) and bare Mg alloy substrate. The 20-400 coating sample was chosen for in vitro cell culture study based on its superior mechanical and corrosion behavior. During optimization of these cell culture studies, the high corrosion rate and greater hydrogen gas evolution from bare alloy surfaces created problems in in vitro experiments. Hydrogen gas evolution and an increase of pH due to the high corrosion rate prevented cell adhesion. To overcome this problem, preincubation for both the substrates was done in simulated body fluid, which provides a natural corrosion protection layer.[50] Along with preincubation, the bioactive property of hydroxyapatite has also contributed to the improvement in cell adhesion.[51] After 4 h of incubation, fluorescent images of the cells on the two substrates as well as the control were captured (Fig. 10). The HA-coated surface shows more cells than the bare Mg-alloy surface, indicating better initial adhesion of cells in the former. In fact, the coated surface shows better cell adhesion than controls, which might be due to the presence of an HA coating that attracts osteogenic cells to the surface. The coating of hydroxyapatite also introduces higher corrosion resistance, which prevents physical detachment of cells from the coated alloy surface along with corroded debris.

MTT assay was performed to observe viability of MG-63 cells on bare and coated samples. For these studies, cells were cultured on bare and coated samples for 1 and 3 days (Fig. 11). The viability is found to be 41% higher on coated samples as compared to the bare samples after incubation for 1 day. After day 3 of incubation, a similar 41% higher viability is again noted on the coated samples. The reason for this observation is the presence of HA on the surface, as well as high corrosion resistance, low pH change, and low hydrogen evolution on the coated sample compared with the bare samples. However, a decrease in viability was observed in both the samples at day 3 compared with day 1. The probable reason could be the competition between cell proliferation and a slow rate of corrosion and hydrogen evolution. Hence, based on these data, further studies on long-term cell incubation and

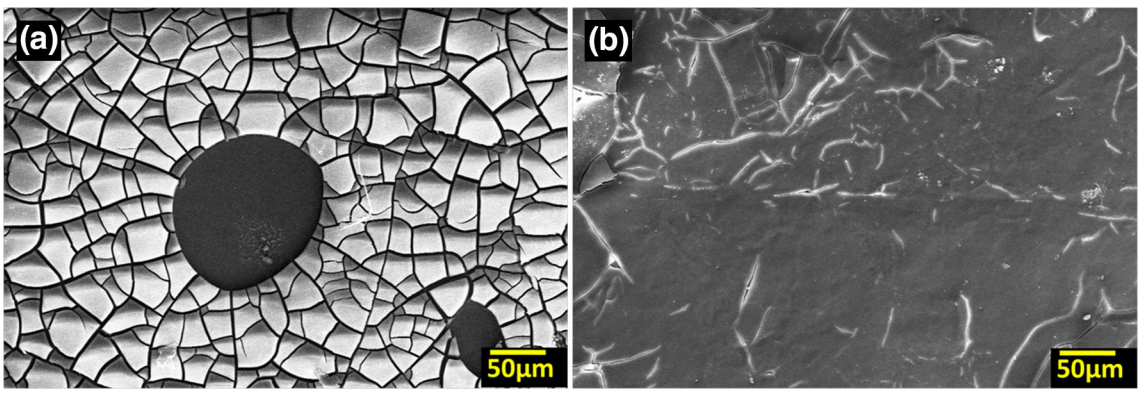

Fig. 9. SEM micrographs after corrosion of (a) bare Mg-3Zn alloy and (b) HA coated Mg-3Zn alloy sintered at 400°C.

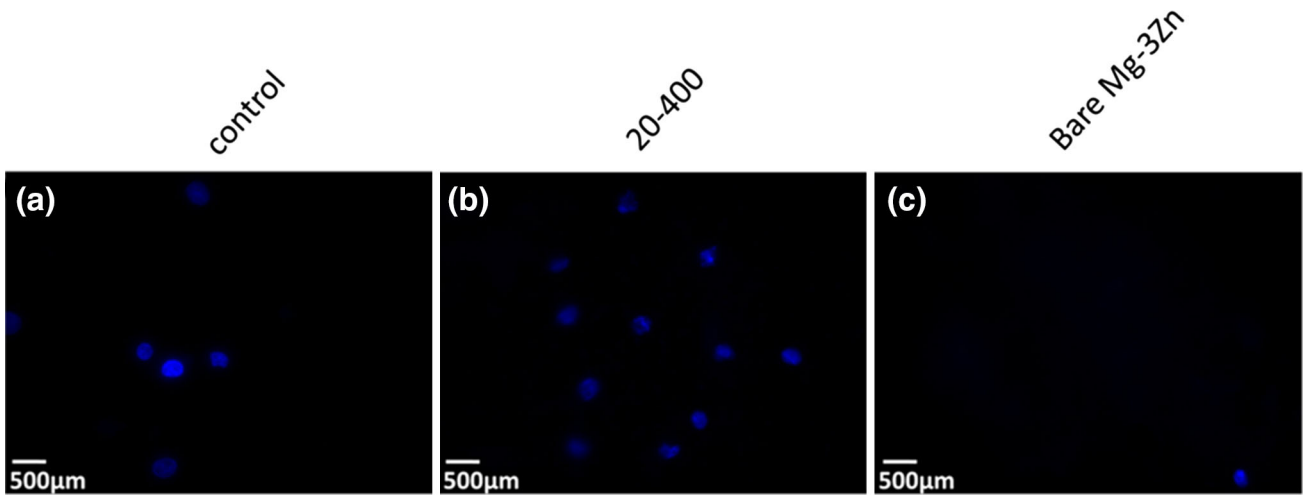

Fig. 10. Fluorescence images of (a) control, (b) HA coated Mg-3Zn, and (c) bare Mg-3Zn samples, seeded with MG-63 cells for 4 h.

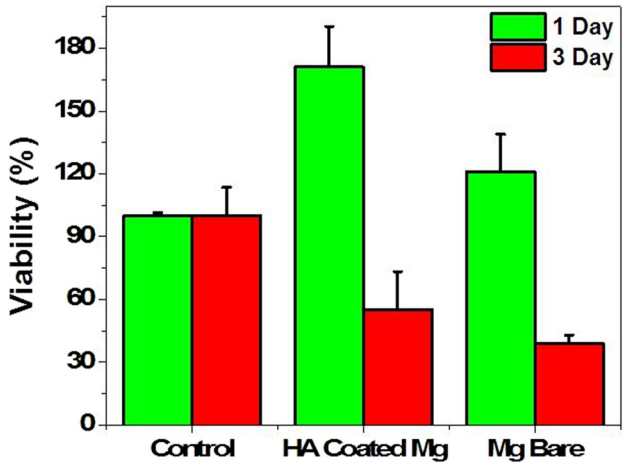

Fig. 11. Cell viability expressed as a percentage of the viability with respect to control (considered as 100%) after 1 and 3 days of incubation in bare Mg-3Zn alloy and HA-coated Mg-3Zn.

assessment is warranted, which would give more insight into the biocompatibility of this material system.

CONCLUSION

In the current study, the sol–gel coating of hydroxyapatite was done successfully on a Mg-3Zn alloy. It is found that the surface roughness has a significant effect on the morphology and homogeneity of the coating. The substrate with lower roughness produces a uniform coating with fewer cracks. The mechanical properties of the coatings are found to be best at lower roughness and higher sintering temperature. The corrosion resistance of the HA coating increases with the increase in sintering temperature and shows a 40-times improvement over the bare Mg alloy surface. The HA-coated Mg surface shows a significant improvement in osteogenic cell adhesion and viability, which is impressive considering its potential application in orthopedic implants.

ACKNOWLEDGEMENTS

The authors are grateful to all the laboratory stuff at Metallurgical and Materials Engineering Department and Centre of Nano Technology, Indian Institute of Technology, Roorkee for their facilities. The authors would like to thank Mr. Khelendra Agarwal for his support during the experiments.

REFERENCES

1. T. Kraus, S.F. Fischerauer, A.C. Hänzi, P.J. Uggowitzer, J.F. Löffler, and A.M. Weinberg, *Acta Biomater.* 8, 1230 (2012).
2. M.P. Staiger, A.M. Pietak, J. Huadmai, and G. Dias, *Biomaterials* 27, 1728 (2006).
3. P.E. DeGarmo, *Materials and Processes in Manufacturing*, 5th ed. (New York: Collin Macmillan, 1979).
4. L. Gibson and M. Ashby, *Cellular Solids. Structure and Properties*, 2nd ed. (Sydney: Pergamon Press, 1988), pp. 1–41.
5. J.W. Choi, Y.M. Kong, H.E. Kim, and I.S. Lee, *J. Am. Ceram. Soc.* 81, 1743 (1998).
6. J. Nagels, M. Stokdijk, and P.M. Rozing, *J. Shoulder Elbow Surg.* 12, 35 (2003).
7. G. Song, *Corros. Sci.* 49, 1696 (2007).
8. Z. Li, X. Gu, S. Lou, and Y. Zheng, *Biomaterials* 29, 1329 (2008).
9. F. Witte, V. Kaese, H. Haferkamp, E. Switzer, A.M. Lindenberg, C.J. Wirth, and H. Windhagen, *Biomaterials* 26, 3557 (2005).
10. B.A. Shaw, *Corrosion: Fundamentals, Testing and Protection*, Vol. 13A, ed. D. Stephen (London: ASM International, 2003), p. 692.
11. S.S.A. El-Rahman, *Pharmacol. Res.* 47, 189–194 (2003).
12. W. Yang, P. Zhang, J. Liu, and Y. Xue, *J. Rare Earths* 24, 369 (2006).
13. F. Witte, V. Kaese, H. Haferkamp, E. Switzer, A.M. Lindenberg, C.J. Wirth, and H. Windhagen, *Biomaterials* 26, 3557 (2005).
14. H. Tapiero and K.D. Tew, *Biomed. Pharmacother.* 57, 399 (2003).
15. H. Okamoto, *J. Phase Equilib. Diffus.* 15, 129 (1994).
16. H. Haferkamp, F.W. Bach, V. Kaese, K. Möhwald, M. Niemeyer, and H. Schreckenberger, *Magnesium Alloys and Technology*, ed. K.U. Kainer (Weinheim: Wiley, 2003), pp. 226–227.
17. A.F. Lotfabadi, M.H. Idris, A. Ourdjini, M.R.A. Kadir, S. Farahany, and H.R. Baksheshi-rad, *Bull. Mater. Sci.* 36, 1103 (2013).

18. M.P. Staiger, A.M. Pietak, J. Huadmai, and G. Dias, *Biomaterials* 27, 1728 (2006).
19. M. Bohner and J. Lemaitre, *Biomaterials* 30, 2175 (2009).
20. J. Currey, *Nature* 414, 699 (2001).
21. P. Ducheyne and Q. Qiu, *Biomaterials* 20, 2287 (1999).
22. M. Mazaheri, M. Haghighatzadeh, A.M. Zahedi, and S.K. Sadrnezhaad, *J. Alloy Compd.* 471, 180 (2009).
23. S.V. Dorozhkin, *Acta Biomater.* 10, 2919 (2014).
24. L.I. KaiKai, W. Bing, Y. Biao, and L.U. Wei, *Chin. Sci. Bull.* 57, 2319 (2012).
25. M. Tomozawa and S. Hiromotoi, *Mater. Trans.* 51, 2080 (2010).
26. T. Onoki, S. Yamamoto, H. Onodera, and A. Nakahira, *Mater. Sci. Eng. C* 31, 499 (2011).
27. Z. Zhang, G. Zhang, and M. Wei, *J. Biomed. Mater. Res. B* 89, 408 (2008).
28. S. Keim, J.G. Brunner, B. Fabry, and S. Virtanen, *J. Biomed. Mater. Res. B* 96B, 84 (2011).
29. M. Razavi, M. Fathi, O. Savabi, D. Vashaee, and L. Tayebi, *Surf. Eng.* 30, 545 (2014).
30. Y.W. Song, D.Y. Shan, and E.H. Han, *Mater. Lett.* 62, 3276 (2008).
31. M. Razavia, M. Fathi, O. Savabi, D. Vashaee, and L. Tayebi, *Mater. Sci. Eng. C* 48, 21 (2015).
32. H. Tang, T.Z. Xin, Y. Luo, and F.P. Wang, *Mater. Sci. Tech.* 29, 547 (2013).
33. R. Rojaee, M. Fathi, and K. Raeissi, *Mater. Sci. Eng. C* 33, 3817 (2013).
34. A. Roy, S.S. Singh, M.K. Datta, B. Lee, J. Ohodnicki, and P.N. Kumta, *Mater. Sci. Eng. B* 176, 1679 (2011).
35. S. Sonmez, B. Aksakal, and B. Dikici, *J. Alloy Compd.* 596, 125 (2014).
36. E. Milella, F. Cosentino, A. Licciulli, and C. Massaro, *Biomaterials* 22, 1425 (2001).
37. D.M. Liu, Q.Z. Yang, T. Troczynski, and W.J.J. Tseng, *Biomaterials* 23, 1679 (2002).
38. S. Sonmez, B. Aksakal, and B. Dikici, *J. Alloy Compd.* 596, 125 (2014).
39. M.H. Fathi and A. Hanifi, *Adv. Appl. Ceram.* 108, 363 (2009).
40. R. Jenkins and R.L. Snyder, *Introduction to X-ray Powder Diffractometry* (New York: Wiley, 1996).
41. W.C. Oliver and G.M. Pharr, *J. Mater. Res.* 7, 1564 (1992).
42. S. Shadanbaz and G.J. Dias, *Acta Biomater.* 8, 20 (2012).
43. S. Neralla, D. Kumar, S. Yarmolenko, and J. Sankar, *Compos. B* 35, 157 (2004).
44. J.L. Arias, M.B. Mayor, J. Pou, Y. Leng, B. Leon, and M. Perez-Amor, *Biomaterials* 24, 3403 (2003).
45. L. Cleries, J.M. Fernandez-Pradas, and J.L. Morenza, *Biomaterials* 21, 1861 (2000).
46. A.J. Whitehead and T.F. Page, *Solid Films* 220, 277 (1992).
47. G.R. Anstis, P. Chantiklul, B.R. Lawn, and D.B. Marshall, *J. Am. Ceram. Soc.* 64, 533 (1981).
48. L.L. Hench and J. Wilson, *Advanced Series in Ceramics*, Vol. 1, ed. L.L. Hench and J. Wilson (Singapore: World Scientific, 1993), pp. 1–24.
49. H.M. Fathi and A.D. Mohammadi, *Mater. Sci. Eng. A* 474, 128 (2008).
50. R. Willumeit, A. Möhring, and F. Feyerabend, *Int. J. Mol. Sci.* 15, 7639 (2014).
51. J.D. de Bruijn, C.A. van Blitterswijk, and J.E. Davies, *J. Biomed. Mater. Res.* 29, 89 (1995).